Data Products for the OCTL to OICETS Optical Link Experiment

J. Kovalik*, A. Biswas, K. Wilson, M. Wright, T. Roberts
Jet Propulsion Laboratory, California Institute of Technology, Pasadena, CA 91109

ABSTRACT

JPL has developed a series of software and hardware tools to analyze and record data from a 50Mb/s down and 2 Mb/s up bi-directional optical link with the LUCE terminal onboard the LEO OICETS satellite. This paper presents the data products for this experiment including the system architecture and analysis of the actual data received.

Keywords: OICETS, optical communications, data products

1. INTRODUCTION

1.1 OICETS to OCTL Experiment (OTOOLE)

The Jet Propulsion Laboratory (JPL) undertook an experiment in May and June 2009 to perform a bi-directional optical communications link between the Laser Utilizing Communications Equipment (LUCE) payload on the Optical Inter-orbit Communications Engineering Test Satellite (OICETS) and the Optical Communications Telescope Laboratory (OCTL) located at JPL's Table Mountain Facility (TMF) near Wrightwood, California. The experiment was a collaboration between JPL, the National Institute of Information and Communications Technology (NICT) which controlled the optical communications payload and the Japan Aerospace Exploration Agency (JAXA) which controlled the OICETS satellite.

The experiment consisted of 4 separate links that took place on May 21, June 2, June 4 and June 11, 2009. Each link occurred between 3 and 4 o'clock in the morning local time and lasted a few minutes.

The 9 μrad [1] LUCE laser downlink transmitted 80 mW of average laser power with a 50 Mb/s On-Off-Key (OOK) PN 15 Pseudo Random Bit Sequence (PRBS) to the OCTL telescope. The OCTL telescope uplinked a 9 mW total average power 819 nm data signal that consisted of 3 laser beams each with a 1 mrad $1/e^2$ full divergence. The data rate was 2 Mbps and the content was a PN 15 PRBS in binary Pulse Position Modulation (PPM) format. A separate continuous wave (cw) 801 nm beacon with a total power of up to 4 W and 4 separate beams each with a 2-mrad beam divergence was also transmitted from OCTL. The beacon and uplink were transmitted as beamlets through the main 1-m diameter aperture, while the 20-cm diameter acquisition scope was used to receive the downlink. More detailed descriptions and discussions appear in companion papers in this volume.

1.2 Concept of Operations

The ephemeris of the OICETS satellite was obtained from a consolidated predict file (CPF) that was updated before the link and sent to JPL. JPL used this file to generate a state vector file with time, azimuth and elevation that was loaded into the OCTL control computer.

Each link began with OCTL pointing its beacon beam at the OICETS satellite at a pre-determined time. The LUCE terminal would be blind pointing at OCTL during this time. LUCE would acquire the uplink beacon and then transmit its downlink data laser beam to OCTL. OCTL would then transmit its uplink data laser beam to the OICETS satellite. At this point, LUCE would begin fine tracking on the uplink laser signal and the beacon laser signal would be turned off. The bi-directional link would continue until the pre-determined experiment stop time.

2. DATA ACQUISITION SYSTEM HARDWARE

2.1 Data Acquisition Architecture

The overall data acquisition used a Personal Computer (PC) to receive and store both the actual communications signal and a series of ancillary data. LabVIEW software ran all the acquisition programs which allowed both a real time control of the acquisition and also a real time display of the received data. The motivation behind the data acquisition system was to provide information on the quality of the link and the performance of OCTL as a transceiver.

*Joseph.M.Kovalik@jpl.nasa.gov; phone 1 818 393-6397; fax 1 818 393-614

Signal monitor data was recorded at 2 Hz. The downlink signal power was recorded continuously at 5 kHz to provide a sufficient bandwidth to study atmospheric effects like signal fading. A Bit Error Rate Tester (BERT) gave the bit error rate of the downlink data in real time. A high speed digitizer took snapshots of the downlink signal in order to give instantaneous, high speed signal information that could be studied in post processing. All data was time stamped and synchronized to Global Positioning system (GPS) time.

Video of the signal received by the telescope was also recorded to give a visual record of the link. Figure 1 shows a block diagram of the data acquisition architecture.

Figure 1. Block diagram of the data acquisition architecture.

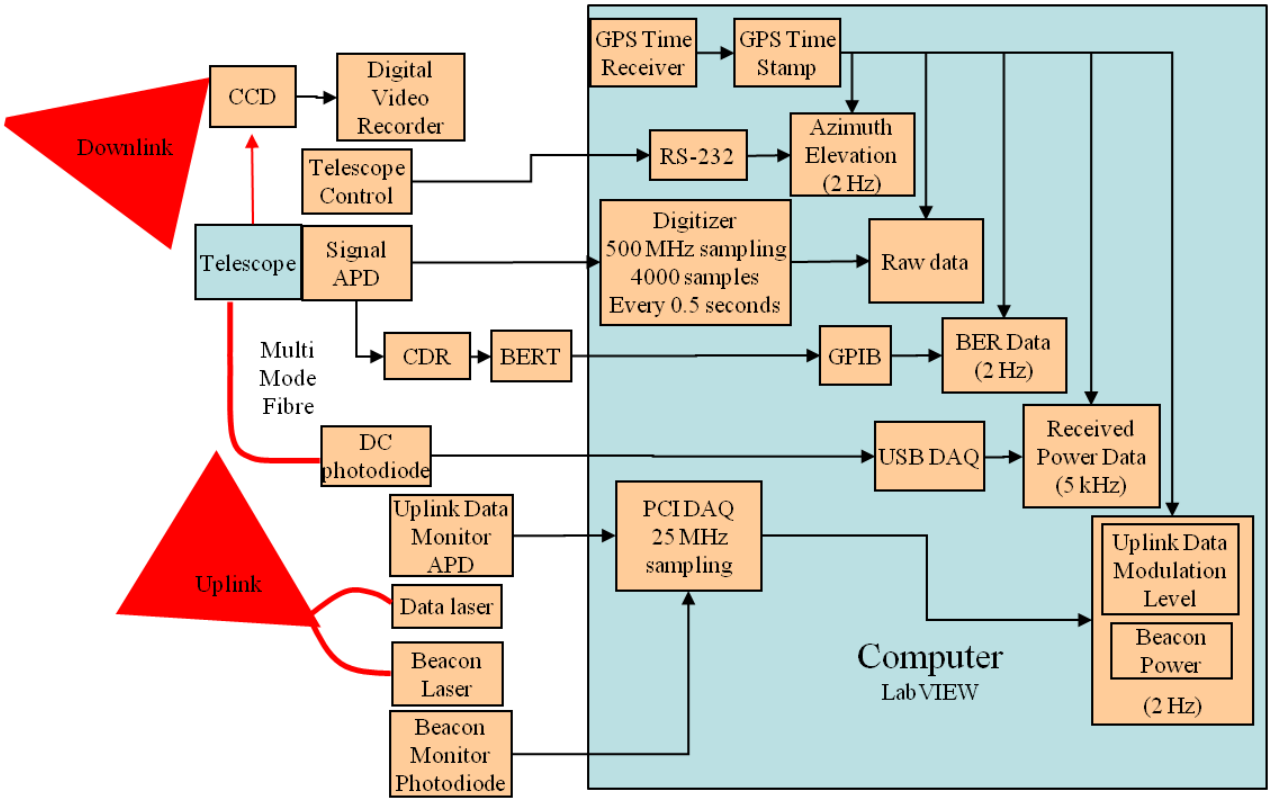

2.2 Uplink Data Generator

The uplink data consisted of a 2 Mbps PN 15 PRBS that was transmitted in a binary PPM format. The PRBS OOK data was generated by a BERT Transmitter and converted to binary PPM by a simple logic circuit shown in figure 2. The output was then amplified and given a DC bias to provide the appropriate current needed to achieve the desired uplink data power.

Figure 2. Logic used to convert OOK PRBS to binary PPM.

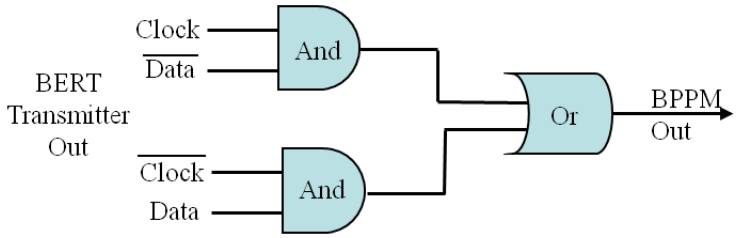

2.3 Uplink Power Monitor

Both the uplink beacon and data power levels were monitored during the pass. A PIN detector with a 5 nm narrowband filter centered at the 801 nm beacon wavelength was aimed at the spot where the 3 uplink beacon lasers were combined. The output of the detector was then calibrated to the transmitted beacon power.

An APD module with a 5 nm narrowband filter centered at the 819 nm uplink data laser wavelength was pointed at the fibre that delivered the laser to the output optics. Again, the output was calibrated in terms of the uplink data power.

Both the beacon and data power levels were sampled at 25 MHz by a PCI based DAQ card. The beacon power was averaged and stored at a 2 Hz rate. The maximum and minimum power levels of the modulated data laser were recorded and then averaged to obtain a modulation level that was stored at a 2 Hz rate.

2.4 Downlink Data Detector

The downlink data was detected by a 3mm APD module with a 100 MHz bandwidth. The output was then split. One signal was sent to a clock and data recovery chip. The clock and data output were then sent to a BERT receiver. The average bit error rate over a 0.5 second interval was determined and transferred to the data computer over a GPIB interface.

The other half of the APD signal was recorded directly by PCI based digitizer at 500 MHz. Every 0.5 seconds, the digitizer would record a 4000 samples of data and then store it on the data computer.

2.5 Downlink Signal Monitor

The optical receiver assembly receiver split the signal light onto two separate paths. One went directly to the APD. The other was directed into a 200 µm multi-mode fibre that led into the coudé room. A PIN detector measured the fibre output power and sent the signal to a USB based DAQ that sampled continuously at a 5 kHz rate. This fast data was buffered and streamed to disk. The power level was also averaged over a 0.5 second interval and then stored as part of the monitor data.

2.6 Telescope Pointing

The telescope control computer outputs the actual measured azimuth and elevation of the gimbal though an RS 232 interface. This was recorded at 2 Hz by the data computer so that any anomalies in pointing could be checked during post processing.

2.7 Video Signal Recorder

The optical receiver assembly had a channel that allowed a CCD video camera to detect the downlink signal. A digital video recorder then recorded the image channel together with audio of the control room for the entire duration of the link.

On some of the passes, a fisheye lens coupled to a CMOS camera took subsequent images of the whole sky during the link. These images were then stitched together to make an accelerated time lapse movie of the link.

3. DATA ACQUISITION SYSTEM SOFTWARE

3.1 Graphical User Interface

A graphical user interface that allowed real time control of the data acquisition system and visualization of the received data can be seen in figure 3. A series of LabVIEW programs were written to control and verify the status of each data acquisition channel. A supervisory program would collect the various channels of 2 Hz data and store it to file. An updated display of ephemeris data including satellite range, azimuth and elevation together with a plot of the actual telescope elevation superposed on the overall elevation profile gave a graphical indication of the satellite's position.

3.2 Data Files

A single ASCII data file for the 2 Hz data was generated during each run. The data records included: GPS time, Azimuth, Elevation, Uplink Data Modulation Power, Beacon Power, Mean Received Power and Bit Error Rate.

A single ASCII data file for the 5 kHz sampled data was also produced. The data was buffered in half second intervals and includes the time stamp for each buffer.

Finally, a set of unsigned 8 bit data files for the 500 MHz data was created. Each data file was given a name with a timestamp and a range of the digitizer ADC that was necessary for rescaling the data to volts.

Figure 3. Graphical User Interface for data acquisition monitor and control

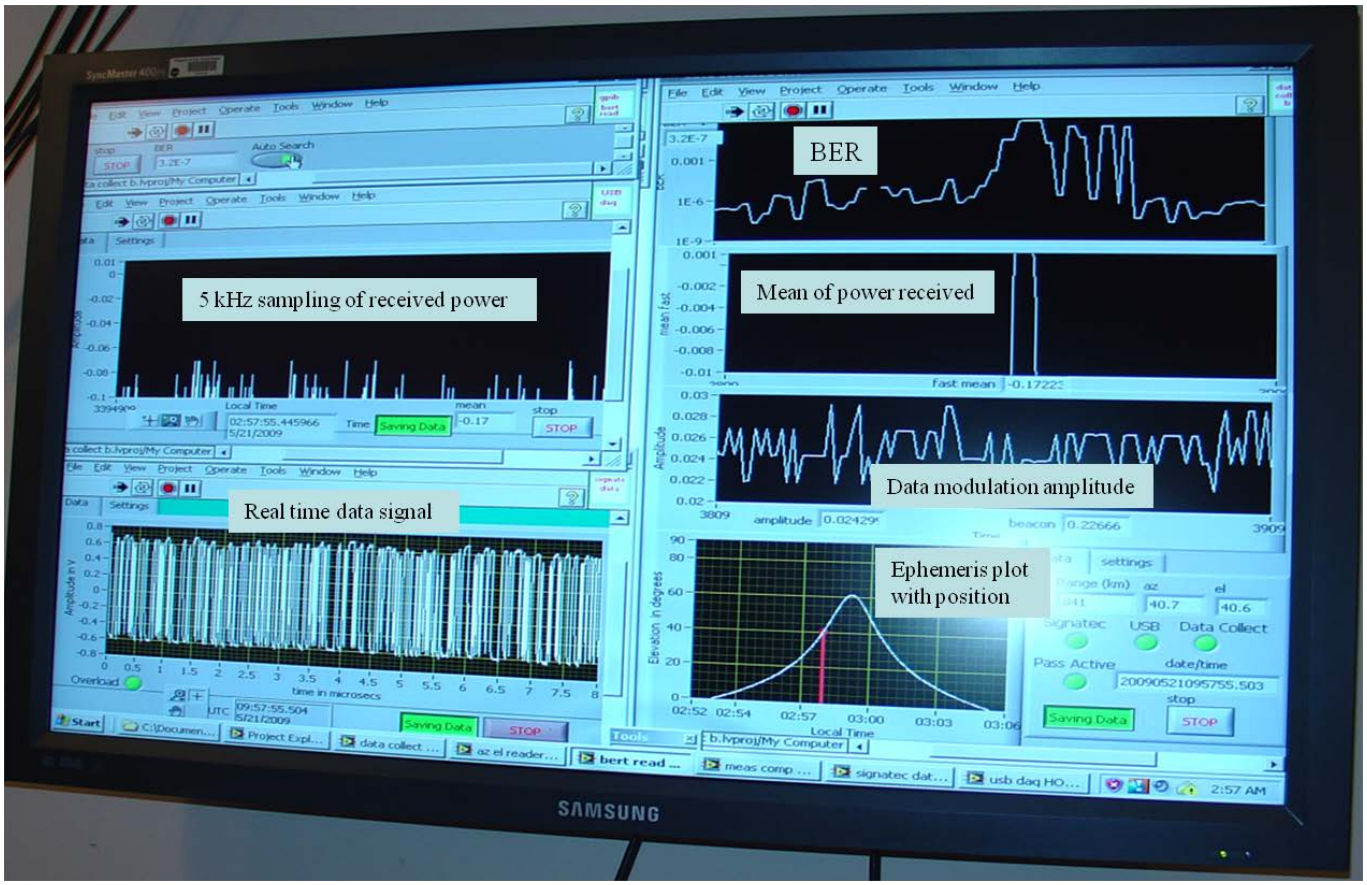

4. EXPERIMENTAL RESULTS

4.1 Overview of Link

While a total of four separate links took place, only the results from June 11, 2009 will be presented here. OICETS rose above the horizon at 09:48:37 UTC. The link was scheduled to begin at 9:52:04 UTC when the elevation angle exceeded the 20° tree line around the OCTL site. The pass lasted until 9:54:19 UTC when the LUCE terminal would point near the sun illuminated portion of the Earth. Time t=0 for all subsequent data plots is 09:48:37 UTC.

Figure 4 shows the measured azimuth and elevation of the pass. The telescope did not go through 0° azimuth which could have produced a discontinuity in the link as the telescope would undergo a cable unwrap.

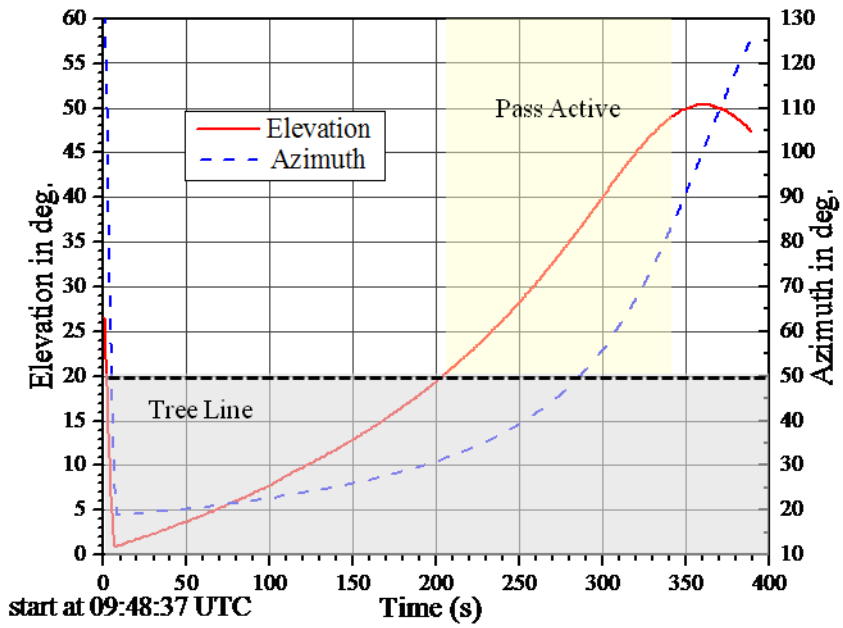

Figure 4. Measured azimuth and elevation for the pass on June 11, 2009

4.2 Received Power Level

The downlink power received from OICETS was predicted using the standard link equation, shown below.

$$P_r = EIRP \times L_s \times \eta_{atm} \times G_R \times \eta_R$$

where the EIRP represents the emitted isotropic radiated power, L_s is the space loss, η_{atm} is the atmospheric attenuation loss, G_R is the receiver gain and η_R is the receiver efficiency. The average transmitted power was 80 mW with a beam divergence of 9 µrad, while the receive aperture diameter was 20 cm with a20% linear obscuration ratio. The variation in L_s and η_{atm} were accounted for in predicting the received downlink power. The atmospheric attenuation loss was determined using the MODTRAN [2] where aerosol models corresponding to rural 23 km visibility and desert extinction were used. For the desert extinction, a measured ground wind speed of 5 m/s was used.

Figure 5 below shows a comparison between the predicted and received laser power averaged for 500 milliseconds. The comparison shows that the atmospheric aerosol models chosen serve as good bounds for the conditions prevalent at the receiving station on June 11, 2009. Similar agreement (not shown) was also obtained on other passes.

The dropouts in received power are due to instabilities in the fine pointing loop and have been seen by other ground stations [1].

4.3 Fast Data

The received downlink signal sampled at 5 kHz was analyzed for fast changes in intensity due to pointing and atmospheric effects. A PSD of the downlink power in Figure 6 shows a small resonance at 16 Hz. Otherwise the spectral content of the data rolls off at about 500-600 Hz which is consistent with power fluctuations due to atmospheric effects [3]. There is also present a forest of peaks with a 67 Hz spacing starting at 300 Hz that is not seen on the detector noise.

The scintillation index as a function of elevation angle was determined from the measured data by choosing short (approximately 4-seconds) time windows. The histogram of the received signal power shows a reasonable, though imperfect agreement with a lognormal distribution. An example for one of the time windows is shown in Figure 7. Figure 8 shows the measured variation of the normalized variance or scintillation index (SI) along with the modeled SI

and its improvement with aperture averaging. The model used the Hufnagel-Valley refractive index structure function, C_n^2 model [3] and aperture averaging reported in ref. [4]. The root mean square wind speed derived from the Bufton model based on measured ground wind speed and the satellite slew-rate was estimated to be 21-24 m/s. However, with this rms wind-speed, the C_n^2 model under-predicts the observed SI. Instead the rms wind speed was used as a free fitting parameter and a good match (figure 9) was found for an rms wind speed of 59 m/s.

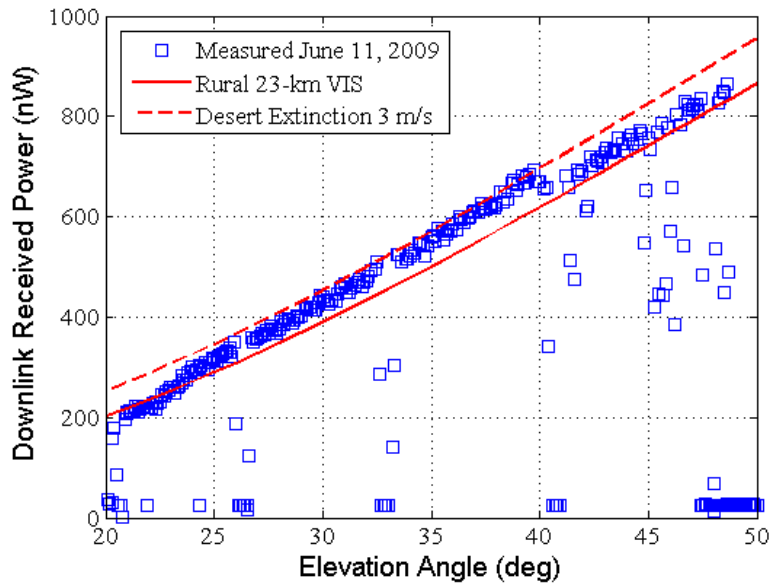

Figure 5. Comparison of measured and predicted downlink received power.

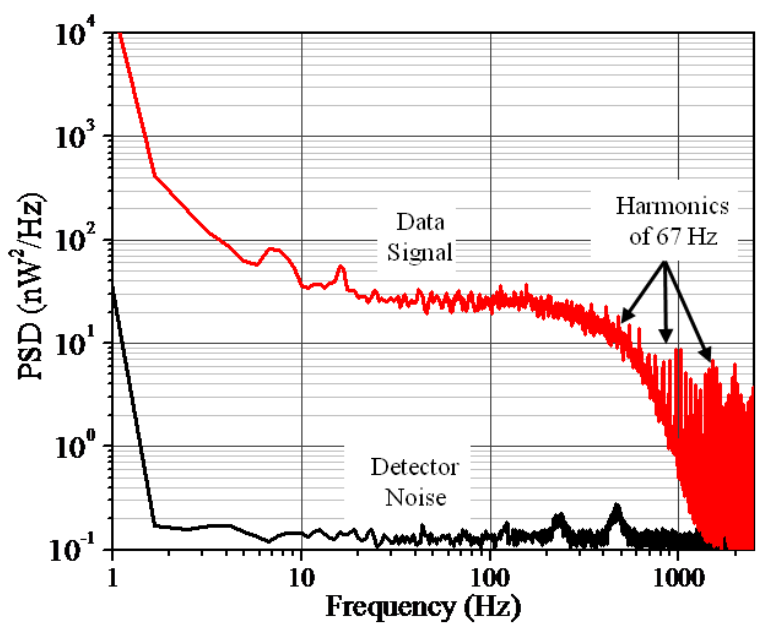

Figure6. Power Spectral density of the downlink signal sampled at 5 kHz.

As an additional check we calculated the r0 for a zenith angle of 70-degrees using this rms wind speed value and obtained a value of r0=7.5 cm. Unfortunately, the r0 was not simultaneously measured at the time of the experiment.

However, TMF site statistics gathered over several months using a differential image motion system has yielded median r0 values of 6 cm varying from 4-10 cm at a zenith angle of 70°. The r0 value of 7.5 cm falls within this range and serves as a sanity check.

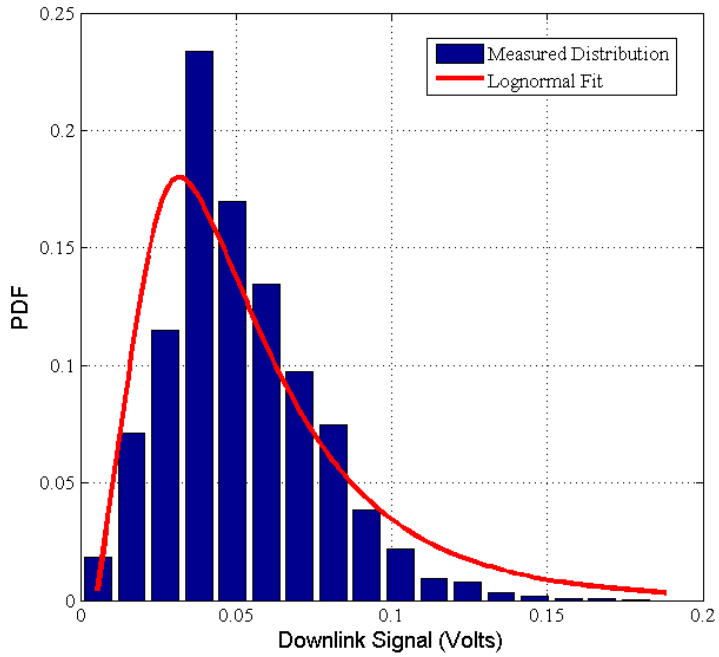

Figure 7. Comparison of the received downlink power histogram to a lognormal distribution

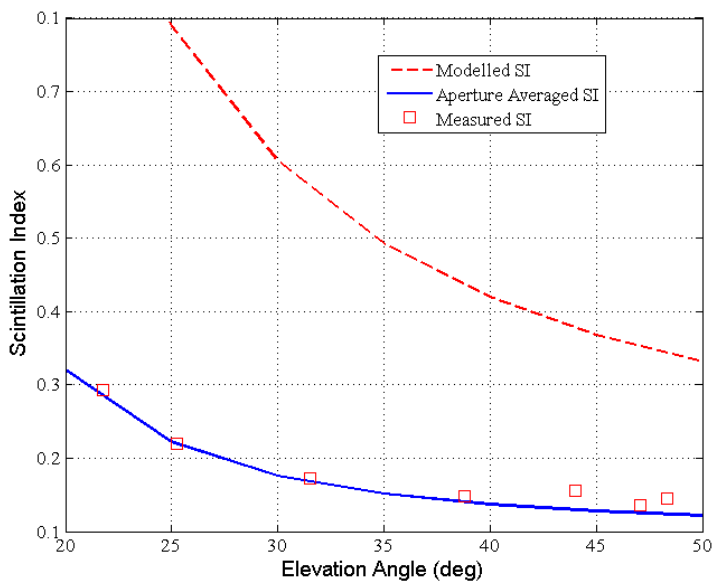

Figure 8. Measured scintillation index (SI) variation with elevation angle measured on June 11, 2009, compared with the aperture averaged SI. The SI without aperture averaging is also shown for comparison.

4.4 Uplink Power Levels

Figure 9 shows a composite plot of the time sequence of signals exchanged between OCTL and LUCE in arbitrary units. The beacon and uplink data lasers transmitted from OCTL are turned on as OICETS approaches the horizon. Once a downlink was detected at OCTL, the power level on the beacon was reduced in steps until it was turned off. Figure 9 also shows power levels detected by the LUCE terminal. The coarse sensor signal builds up as the spacecraft rises and then drops off as the beacon is turned down. The fine pointing sensor is clearly saturated as the link is acquired. Unexpectedly, the fine pointing sensor appears to recover from saturation as the beacon power is turned down. The fine-pointing sensor signal also shows dropouts synchronously with the downlink whereas the coarse pointing sensor does not which confirms that the dropouts are related to anomalous behavior in the fine pointing loop.

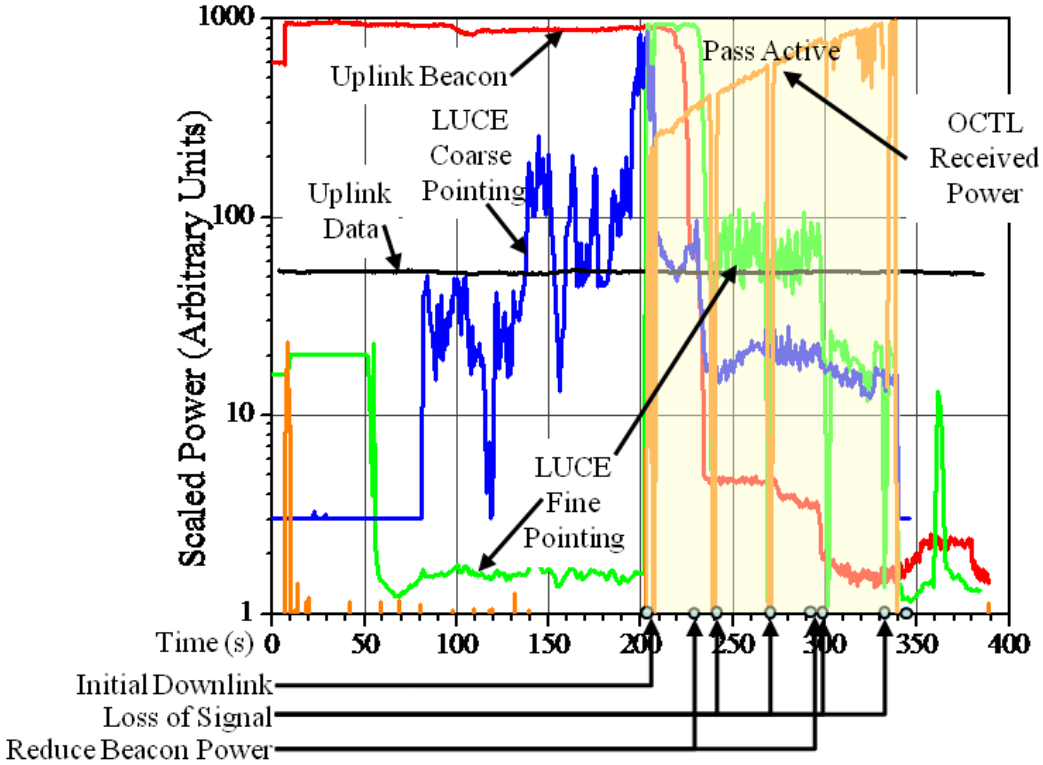

Figure 9. Power levels transmitted from OCTL and detected by the LUCE terminal.

Figure 10 shows a comparison of the received signal at LUCE with link analysis. Here, the elevation angle is plotted against the power in mW. The r0 value inferred from the downlink SI above was wavelength corrected and used in order to approximate the atmospheric Strehl degradation [3] and book-kept as a loss in the link analysis used to predict power received at LUCE. The uplink and beacon receiver losses were taken from ref. 1. The predicted beacon signal variation is consistent with the measurements. In absolute terms, the agreement is within a factor 2-3 except at very low elevation angles where the weak scintillation approximations used in the analysis may fail. The uplink data predicted values are consistently lower than measurements until the beacon is turned off when they appear to merge. This again suggests that the beacon light was illuminating the fine sensor.

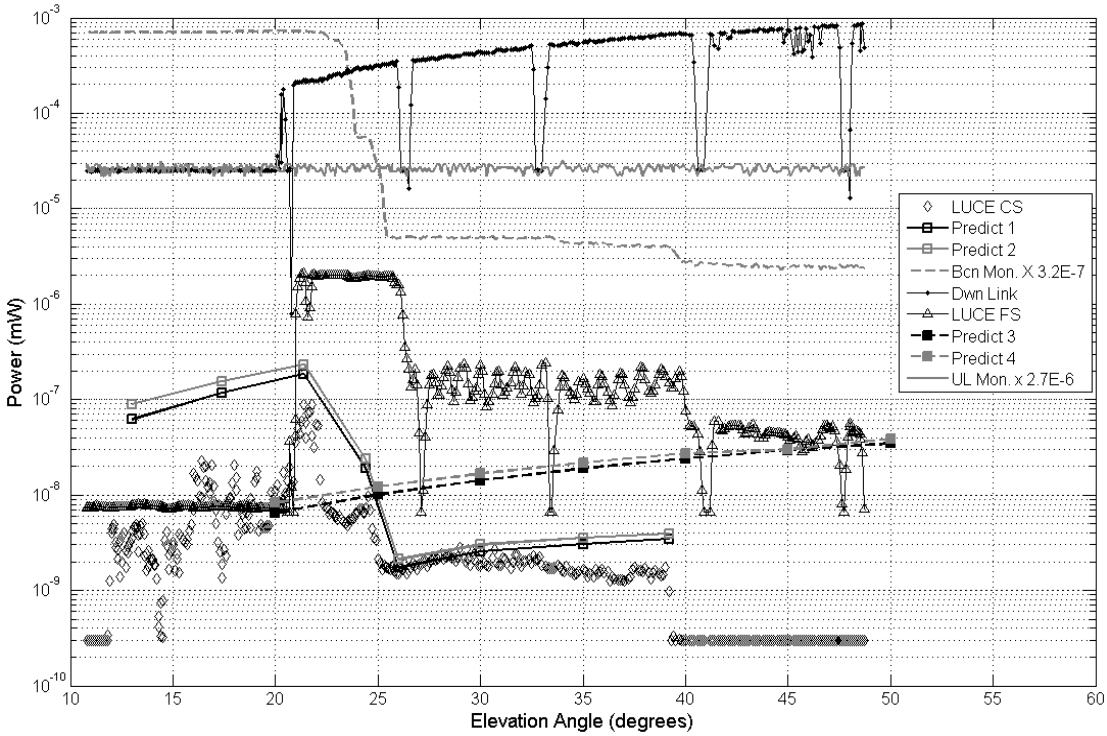

Figure 10. The signals are plotted in terms of received and transmitted power along with the predictions from analysis. (CS-coarse sensor; FS fine sensor; Predict 1&2 are for 801 nm beacon and Predict 3&4 are for the 819 nm data uplink).

4.5 Raw Data

The raw data can be seen in the left hand image in figure 11. The individual bits are clearly visible and the signal is saturating the APD. The right hand image shows a reconstructed eye diagram from the raw data. The eye is clearly open and indicates an optimal bit error rate

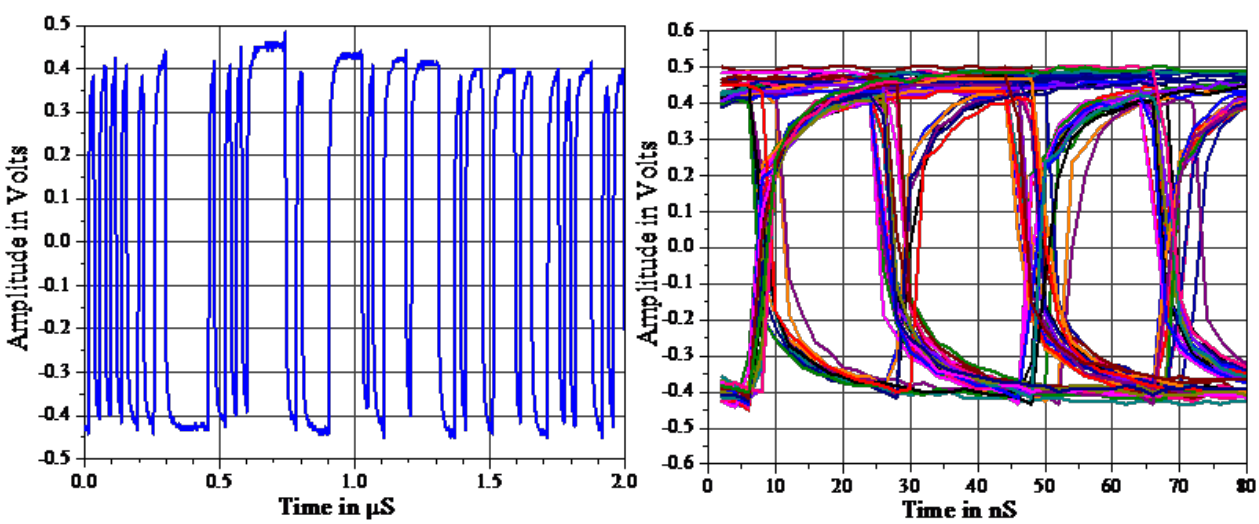

Figure 11. The plot on the left shows raw sampled downlink data. The plot on the right shows a reconstructed eye diagram of the raw data.

4.6 Bit Error Rate

The clock and data recovery system would rapidly lock onto to the downlink signal and provide signal to the BERT. This can be seen clearly in figure 12 where the bit error rate falls significantly below 0.5 whenever light is received. The bite error rate nominally stayed below 10^{-5} for the first part of the pass and 10^{-4} for the second part of the pass. There were always some errors detected even if the signal level was sufficiently high to imply an effective 0 bit error rate given the finite sample length.

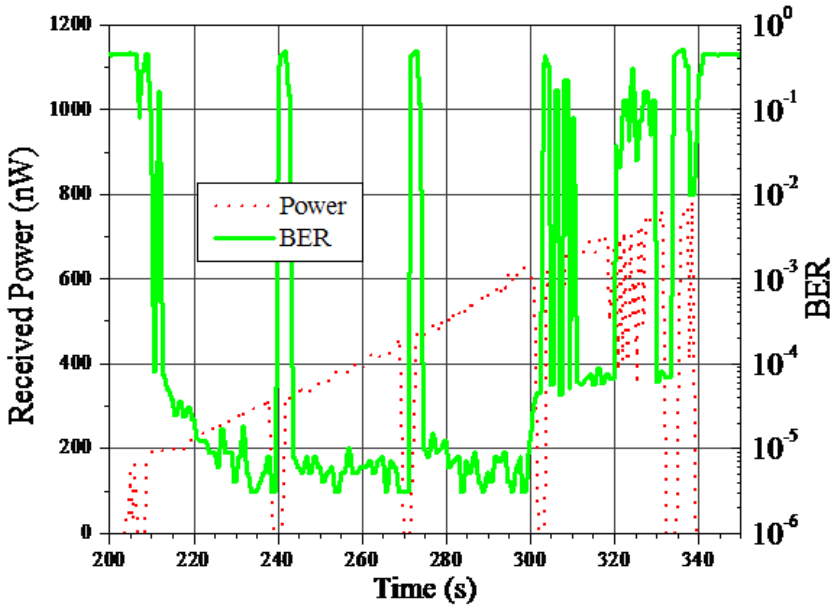

Figure 12. Received power and Bit Error Rate

4.7 Video

Figures 13 and 14 show whole sky and narrow field still images respectively of the OICETS pass. The left hand image in figure 13 shows the beacon laser illuminating trees as OICETS rose above the horizon. The right hand image shows the downlink signal after acquisition had been completed and the full bi-directional communications link had been established.

The four images in figure 14 show the progression of the link as seen by the receiver telescope. The upper left hand image shows a sunlit satellite which verifies the blind pointing of OCTL. The next image on the upper right shows an initial glint of the downlink laser. The subsequent image on the lower left shows that the LUCE terminal is beginning to lock onto the beacon. At this point, the uplink beacon laser is still on. The final image shows the full acquisition with fine pointing locking the terminal to the uplink data laser and the uplink beacon laser turned off.

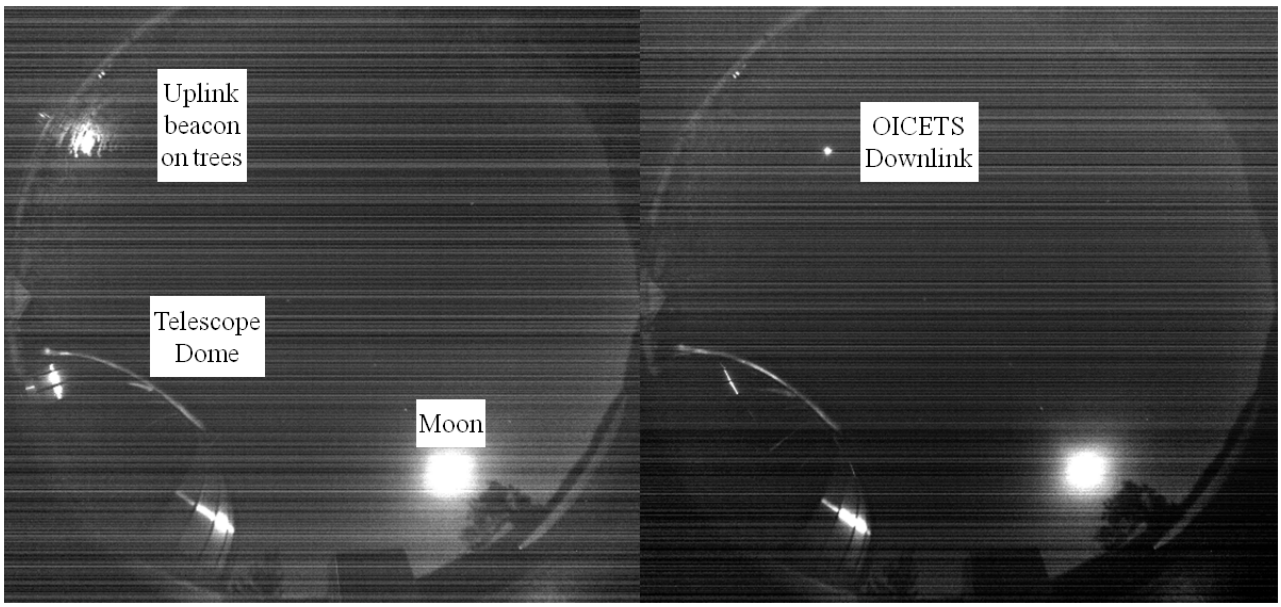

Figure 13. Fisheye lens images of whole sky during an OICETS pass.

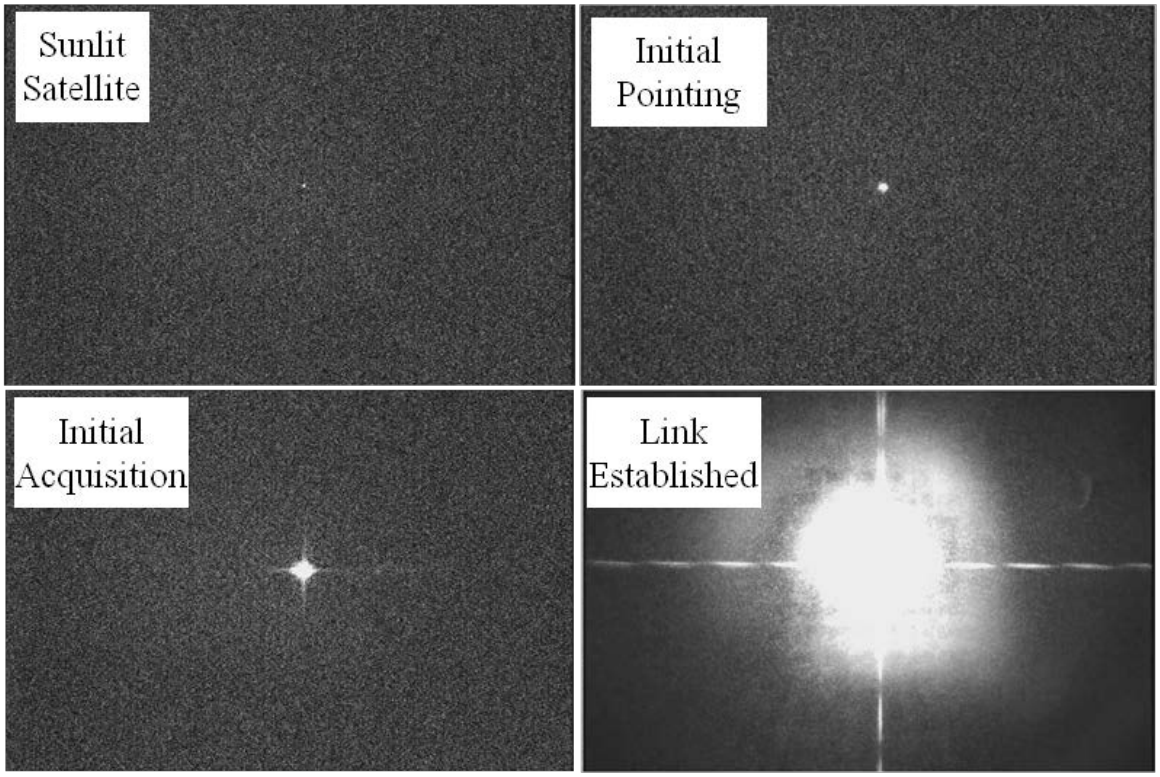

Figure 14. Video capture of OICETS pass taken from 20 cm receive aperture.

5. CONCLUSIONS

JPL developed a series of data products for a series of optical communications links with the OICETS satellite in May and June, 2009. These allowed real time visualization of the link performance and also stored relevant data for later analysis. Initial analysis of the data shows good agreement for the predicted power budget for the both the uplink and downlink.

ACKNOWLEDGEMENTS

The work described here was performed at the Jet Propulsion Laboratory (JPL), California Institute of Technology under contract with the National Aeronautics and Space Administration (NASA).

REFERENCES

[1] Morio Toyoshima, Takashi Takashi, Kenji Suzuki, Shinichi Kimura, Kenichi Takawa, Toshiaki Kuri, Werner Klaus, Mashiro Toyoda, Hiroo Kunimori, Takashi Jono, Yoshihisa Takayama, and Katsuyoshi Arai, "Results of Phase-1, Phase-2 and Phase-3 Kirari Optical Communication Demonstration Experiments with the NICT optical ground station (KODEN), 25th AIAA International Communications Satellite Systems Conference, AIAA 2007-3228, 2007.

[2] A. Berk, G. P. Anderson, P. K. Acharya, J. H. Chrtwynd, L. S. Bernstein, E. P. Shettle, M. W. Matthew and S. M. Adler-Golden, "MODTRAN User's Manual, " Air Force Research Laboratory, Space Vehicle Directorate, Air Force Materiel Command, Hanscom AFB, Massachusetts, August 1999.

[3] L. C. Andrews, R. L. Phillips, "Laser Beam Propagation through Random Media, "SPIE Optical Engineering Press, Bellingham, WA, USA, pp.190-191, pp. 225-226, pp. 282, 1998.

[4] H. T. Yura and W. G. McKinley, "Aperture Averaging of scintillation for space-to-ground optical communication applications, " Applied Optics, 22, 1608-1609, 1983..